JOURNAL OF GEOPHYSICAL RESEARCH, VOL. 102, NO. D24, PAGES 29,205–29,212, DECEMBER 26, 1997

Radiosonde boundary layer budgets above a boreal forest

Alan G. Barr
Atmospheric Environment Service, Saskatoon, Saskatchewan, Canada

Alan K. Betts
Atmospheric Research, Pittsford, Vermont

Abstract. Daytime surface sensible and latent heat fluxes were estimated above boreal forest from the boundary layer budgets of heat and water vapor. Two budgets were integrated from serial soundings in the atmospheric boundary layer: one for the mixed layer and one for the entrainment layer. Horizontal and vertical advection were derived from synoptic analyses. The surface fluxes were then calculated as a budget residual. The mean entrainment parameter A_R above the boreal forest was estimated to be 0.21. The dependence of entrainment on buoyant and shear forcings agreed with earlier studies.

1. Introduction

Daytime surface fluxes of sensible and latent heat drive the growth and development of the mixed atmospheric boundary layer (BL) over land. As the mixed BL deepens, it entrains or mixes downward warmer, drier air from above. The balance between the surface fluxes and entrainment determines the rates of BL deepening, warming, and moistening (or drying).

This study analyzes radiosonde data collected during the 1994 field phase of the Boreal Ecosystem-Atmosphere Study (BOREAS). One of the objectives of BOREAS was to quantify the interaction between the boreal forest and the atmospheric BL and provide data sets to test and improve global forecast and climate models. The diurnal BL cycle is difficult to simulate in large-scale models because the surface forcings are not easily estimated at regional scales and because our understanding of BL-top entrainment is limited. The common parameterizations of entrainment have not been adequately evaluated for different land surface types and wind shears and over the seasonal cycle. Recently, simple BL parameterizations, which better represent entrainment, have been introduced into two global models [*Beljaars and Betts*, 1993; *Hong and Pan*, 1996]. The improved representation of the BL, when coupled to a more interactive land-surface scheme, has led to improvements in forecast skill [*Beljaars et al.*, 1996; *Hong and Pan*, 1996].

Radiosonde-based budgets of heat and moisture provide a framework for evaluating surface and entrainment fluxes at the regional scale and for assessing their joint influence on BL development. *Betts and Ball* [1994] demonstrated good agreement between sonde-based budget estimates of entrainment and direct measurements by instrumented aircraft above the Konza prairie [*Betts et al.*, 1992]. *Diak and Whipple* [1994] used a simple mixed-layer model, driven by sonde-based measurements of BL growth, to estimate daytime surface sensible and latent heat fluxes. *Kustas et al.* [1995] showed how upper air budget methods could be coupled with remotely sensed net radiation and soil heat flux to estimate the surface energy balance. *Betts and Barr* [1996], using the same methodology as here, reevaluated entrainment over the First International Satellite Land Surface Climatology Project (ISLSCP) Field Experiment (FIFE) grassland, and its dependence on wind shear. In this study, we estimate regional surface and entrainment fluxes from the BL budgets of heat and water vapor.

Paper number 97JD01105.
0148-0227/97/97JD-01105$09.00

2. Data

This study analyzes data from the BOREAS southern and northern study areas (SSA and NSA), collected during the three 1994 Intensive Field Campaigns (IFC 1, May 24 to June 16; IFC 2, July 19 to August 8; and IFC 3, August 30 to September 19). A companion paper [*Barr et al.*, this issue] shows the location and land cover of the study areas.

2.1. Upper Air Soundings

Serial upper air soundings were released from Candle Lake (53.73°N, 105.27°W, 503 m, in the SSA) and Thompson (55.75°N, 97.87°W, 206 m, in the NSA) at approximately 1115, 1315, 1515, 1715, 1915, 2115, and 2315 UTC on most days in IFC 1 and 2. Many days in IFC 3 excluded the 1315 sounding because of the later sunrise. The SSA sonde release site was a 200 m wide grassy clearing, 1.5 km south of Candle Lake. It was surrounded by 12–15 m tall mixed forest. The NSA sonde release site was at the zoo near Thompson, on the edge of town near the wooded banks of the Burntwood River.

The radiosondes measured atmospheric pressure, temperature, relative humidity, wind speed, and wind direction at a mean vertical resolution of 27 m (2.9 hPa) in the BL. The mean sonde ascent rate within the BL was 5.4 m s^{-1}. Both upper air sites used Vaisala RS80 radiosondes, equipped with a capacitive bead thermistor and Humicap thin wall capacitor hygristor. The sondes were tracked by a Digicora II MW15 receiver with NAVAID Loran C wind finding. Sonde relative humidity (RH) was corrected for a calibration bias (see appendix). The maximum bias was found at 70% RH, where the sonde sensor underestimated RH by 5%.

2.2. Net Radiation

Net radiation R_n was measured at two BOREAS surface weather stations in each study area: the SSA old aspen and old jack pine tower flux sites, and the NSA old jack pine tower flux site and a site near the Thompson airport. We applied two small adjustments to R_n: a correction for calibration errors and

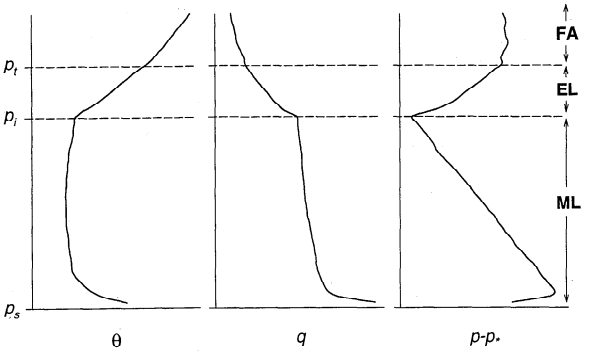

Figure 1. Delineation of the mixed atmospheric boundary layer (ML), entrainment layer (EL), and free atmosphere (FA), as illustrated by the southern study areas 1715 UTC composite sounding.

an adjustment for local versus regional albedo differences [*Barr et al.*, this issue].

2.3. Canadian Regional Finite Element Model Data

Estimates for horizontal and vertical advection, which cannot be determined from serial sonde ascents, were based on regional finite element (RFE) model synoptic analyses, every 3 hours. Because these estimates lacked mesoscale detail on hourly timescales, they added noise to the individual 2-hour BL budgets. However, we believe that the synoptic advection estimates were satisfactory, when averaged over periods of at least 15 days. On this long timescale, the mean horizontal advection was small.

3. Boundary Layer Development

3.1. Delineating the Boundary Layer

For each sounding, we delineated the mixed layer (ML) and entrainment layer (EL), within the atmospheric boundary layer (BL), by visual inspection (see Figure 1). The procedure, although somewhat subjective, used well-defined criteria. The ML top was identified as the lowest level of an inversion in potential temperature θ, which capped a mixed layer of nearly uniform θ. It was also characterized by an abrupt drop in mixing ratio q. We also calculated the profile of saturation pressure p^* [*Betts*, 1982], the pressure of the lifting condensation level of air parcels. The profile of $p_s - p^*$, where p_s is surface pressure, has a distinct local minimum at ML top. The nocturnal BL top was identified as the level that capped a strong surface inversion in θ. It was also characterized by inflections in one or more of the profiles of q, $p_s - p^*$, and horizontal wind speed. The EL top was delineated as the level where the relatively constant free atmosphere (FA) lapse rates in θ, q, and $p_s - p^*$ were reached (Figure 1). This EL top was somewhat more difficult to identify than the ML top. However, precise delineation of EL depth was not critical because the EL budget analysis assumed a constant value of EL depth, equal to its mean depth.

Table 1 lists the sonde analysis days. We analyzed fair-weather days only, excluding days with fewer than six soundings, more than 2 mm of precipitation, low solar irradiation ($R_s/R_{sx} < 0.4$, where R_s/R_{sx} is the ratio of measured daily solar irradiation to the theoretical top-of-the-atmosphere value), substantial horizontal sensible or latent heat advection in the ML, little ML growth (daily maximum BL depth <100 hPa), or significant BL decline (>40 hPa between soundings) during the normal ML growth period (1515–2115 UTC). This left 9, 13, and 10 days in the SSA during IFC 1, 2, and 3, respectively, and 10, 7, and 7 days in the NSA during IFC 1, 2, and 3, respectively.

The data were stratified by study area, IFC, time of day, wind speed and direction, and wind shear across the EL. The effect of wind direction in the SSA is shown in the companion paper [*Barr et al.*, this issue].

3.2. Boundary Layer Development

Composite SSA and NSA sounding time series were prepared by averaging the soundings at each release time. The composites were not used in the BL budget analysis but were prepared to show ML growth over the forest. Within the ML, we first scaled individual profiles of potential temperature θ and mixing ratio q to the mean ML depth, and then averaged the profiles. Above the ML, the pressure coordinate of individual soundings was shifted to match the composite ML top. Because there was no 1315 UTC sounding in IFC 3, 1315 was excluded from the composite sounding time series.

Figures 2 and 3 show the SSA and NSA composite sounding time series. Early morning soundings had a well-developed nocturnal BL, 0.1–0.7 km in depth, which gave way to mixed-layer development, typically by 1515 UTC. The ML then deepened and warmed during the day. A strong superadiabatic zone underlay the ML. The superadiabatic surface layer was deepest (13 hPa on average) at 1515 and 1715 and declined to 9 hPa at 1915 and 2115. Early morning ML growth was slow under the strong nocturnal inversion. By midmorning, ML growth had eroded the nocturnal BL. This led to a period of explosive BL growth as the ML overtook the residual of the previous day's ML. The 1515 ML was deeper in the NSA (pressure depth of 55 hPa) than the SSA (32 hPa) because the Sun rose about 30 min earlier in the NSA. Mean daily maximum ML depth was slightly higher in the NSA (192 hPa) than the SSA (179 hPa) and in IFC 1 (208 hPa) than IFC 2 and 3 (166 and 178 hPa).

ML potential temperature θ was nearly "well mixed" at 1515, 1715, 1915, and 2115 UTC (Figures 2a and 3a). The 1515–2115 θ profiles had a characteristic weak minimum in θ near the midpoint of the ML. By 2315, the minimum θ was nearer to the surface, at 30% of the ML depth. In contrast, ML humidity structure was not "well mixed"; the mixing ratio q declined with height in the BL (Figures 2b and 3b). The mean decline in q from the top of the surface superadiabatic layer to the top of the ML was 0.3 g kg^{-1} at 1515 UTC, 0.7 g kg^{-1} at

Table 1. Days Used in the Sonde Budget Analysis and in Preparing Composite Soundings

IFC	Southern Study Area	Northern Study Area
1	May 25–27, 31, June 1, 4, 6–7, 10	May 25, 27, June 2, 4, 7–10, 13, 16
2	July 21, 23–27, 30–31, Aug. 2–5, 8	July 21, 27, 29, Aug. 1, 4, 5, 8
3	Aug. 31, Sept. 1–2, 6–7, 11, 13, 16–17, 19	Aug. 30, Sept. 1–3, 7, 9, 12

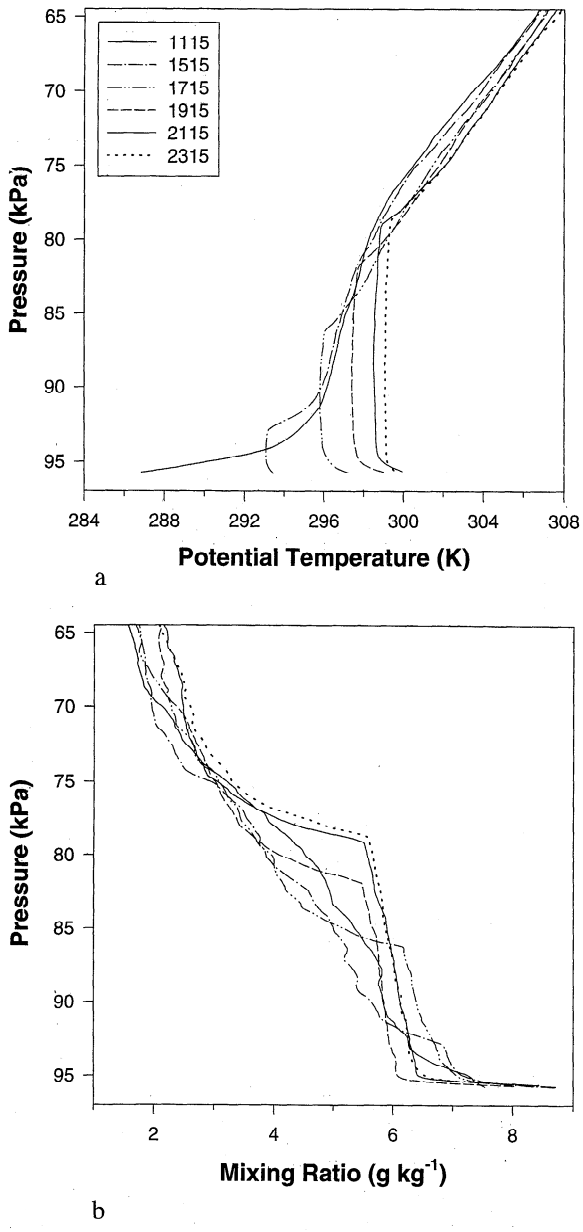

Figure 2. Composite southern study area serial soundings: (a) potential temperature and (b) mixing ratio.

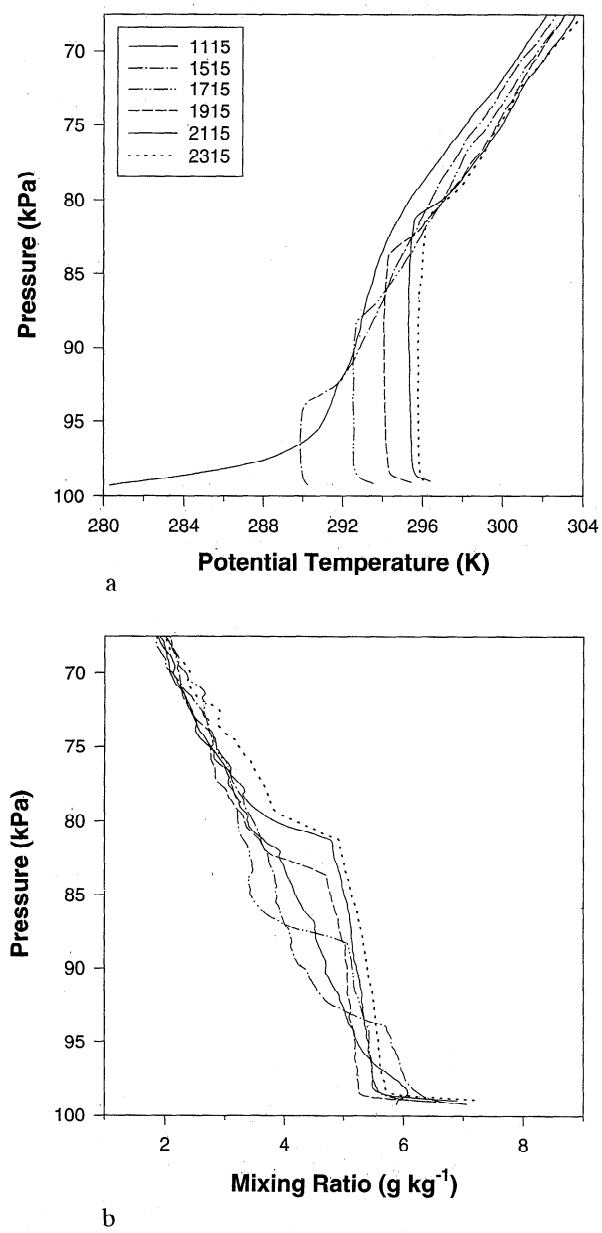

Figure 3. Composite northern study area serial soundings: (a) potential temperature and (b) mixing ratio.

1715 and 1915, and 0.9 g kg^{-1} at 2115. The ML θ and q structures were consistent with other observational studies [*Mahrt*, 1976; *Betts and Ball*, 1994] and large eddy simulations [*Wyngaard and Brost*, 1984].

The EL deepened slightly during the ML growth period (1515–2115 UTC), from a minimum depth of 21 hPa at 1515 to a maximum depth of 33 hPa at 1915. The 1515–2115 mean EL depth was 29 hPa. The composite sounding time series also showed a characteristic zone of cooling near the BL top, produced by overshooting thermals [*Betts*, 1974; *Mahrt*, 1979]. The BL-top cooling zone was partially obscured by subsident warming but was evident when consecutive pairs of soundings were compared.

In both composites (Figures 2b and 3b), ML q fell about 1 g kg^{-1} during the morning hours to a minimum at 1915 UTC, and then increased. The upward transport of moisture can be seen as the BL deepens into drier air above. The composite sounding time series also showed warming and some moistening in the free atmosphere above the BL. Analysis of the RFE model output showed that the free atmosphere warming was dominated by subsidence, horizontal advection, and radiative heating. Shallow cumulus clouds on some days may also transport water out of the BL.

4. Boundary Layer Budget Analysis

4.1. Budget Equations

The analysis follows *Betts and Barr* [1996], with the addition of horizontal and vertical advection from the RFE analyses. We have omitted the equations here. We constructed budgets for the ML and EL for each 2-hour time increment between sondes. The ML equations can be written symbolically for sensible H and latent heat λE as the sums

Table 2. Mean Mixed-Layer Budget Estimates and Their Components, Stratified by Study Area and IFC

			Local Change		Advection		Entrainment		Surface Flux			
	n	R_n	H_l	λE_l	H_a	λE_a	H_i	λE_i	H_s	λE_s	ε_s	β_s
All	56	473	252	−91	3	4	−62	271	192	184	0.96	1.05
SSA	32	488	234	−113	6	4	−74	294	166	185	0.87	0.90
NSA	24	454	275	−60	−1	3	−47	240	227	182	1.09	1.24
IFC 1	19	545	299	−104	10	12	−59	284	251	192	0.98	1.31
IFC 2	20	485	210	−68	−3	−10	−43	285	164	207	0.92	0.79
IFC 3	17	380	247	−102	1	10	−88	239	159	148	0.97	1.08

Values are in units of W m^{-2}. SSA, southern study area; NSA, northern study area; IFC, Intensive Field Campaign; n, number of days, with three individual (2 hour) budget analyses per day.

$$H_s = H_l + H_a + H_i \tag{1a}$$

$$\lambda E_s = \lambda E_l + \lambda E_a + \lambda E_i \tag{1b}$$

The local change terms, H_l and λE_l, were derived for each time step from the time change of sonde variables, averaged though the ML. The horizontal advection terms H_a and λE_a (small in the mean) were estimated from RFE analyses in the ML. The entrainment fluxes H_i and λE_i came from a similar budget equation for the EL, where we also estimated vertical advection from the RFE analyses, and neglected fluxes through the EL top [see *Betts and Barr*, 1996]. The EL budget used a mean EL thickness of 30 hPa, equal to its mean depth. We then calculated the surface Bowen ratio β_s as

$$\beta_s = H_s/\lambda E_s \tag{2}$$

4.2. Surface Energy Balance Closure

The measured surface net radiation R_n (with a small correction for landscape albedo [*Barr et al.*, this issue] was compared with the sum of the surface fluxes derived from the sonde budget. We defined a fractional surface energy balance closure ε_s as

$$\varepsilon_s = (H_s + \lambda E_s)/(R_n - S) \tag{3}$$

where S is the sum of the minor energy balance terms (soil or open-water heat flux, canopy heat storage, and photosynthetic energy flux). A value for ε_s of 1.0 indicates perfect agreement between the sum $H_s + \lambda E_s$ and surface available energy $R_n - S$. A key uncertainty at the regional scale is estimating S, which is primarily a measure of heat storage by the landscape, including photosynthesis. Our best estimate was $S \approx 0.17R_n$ for both the SSA and NSA [*Barr et al.*, this issue].

4.3. Budget Components

Table 2 summarizes our estimates for H_s and λE_s and their components in (1a) and (1b) and the two derived parameters, Bowen ratio β_s and fractional energy balance closure ε_s. The budgets were dominated by the local change and entrainment. For each IFC and study area, horizontal advection contributed negligibly (<10%) to the estimates of the surface fluxes. Because the entrainment latent heat flux exceeded the surface flux, the BL dried on average during the day, as seen in the composite figures. Our energy balance closure parameter ε_s gives some indication of the reliability of the budgets. For the full summer's data set, $\varepsilon_s = 0.96$ (with a best estimate of the bulk landscape storage S of 17% of R_n). The smaller data subsets have values of ε_s, indicating errors in the energy balance, as large as 13% (for the SSA composite).

4.4. Surface Bowen Ratio

The mean surface Bowen ratio β_s was 1.05. The surface Bowen ratio was 38% higher in the NSA than the SSA, and there was a substantial midsummer depression in β_s, presumably associated with peak evapotranspiration from deciduous species. More detailed stratifications, which reduced each analysis to less than 15 days, are not shown, as the variability increased with decreasing sample size.

This mean daytime summer β_s near 1.0 over the heterogeneous boreal forest is in sharp contrast to, say, the FIFE grassland, for which daytime summer β_s is ≈0.4 [*Smith et al.*, 1992].

4.5. Variation With Time of Day

Table 3 shows the time-of-day variation in the budget estimates for H_s and λE_s. We have less confidence in these. The time-of-day variation in H_s is well behaved, but the variation in λE_s is not. The implausible values for λE_s at 1715–1915 and 1915–2115 UTC result from anomalously low mixing ratios in the 1915 soundings (Figures 2b and 3b), perhaps the result of a midday radiation error in the sonde humidity measurement. However, the 1715–1915 underestimation and 1915–2115 overestimation of λE_s, were mutually compensating, and the daily latent heat flux totals were little affected. Previous studies [*Barr and Strong*, 1996; *Betts et al.*, 1995; *Teweles*, 1970] reported a similar, anomalous midday depression in q, which they attributed to radiative heating of the RH sensor. Although the manufacturer's specifications [*Vaisala*, 1992] indicated low

Table 3. Mean Mixed-Layer Budget Estimates, Stratified by Time of Day

			Surface Flux		Entrainment				
Time of Day (UTC)	n	R_n	H_s	λE_s	H_i	λE_i	ε_s	β_s	A_R
1515–1715	56	439	139	177	−106	330	0.87	0.79	0.55
1715–1915	56	520	221	83	−40	268	0.71	2.65	0.09
1915–2115	56	462	216	291	−42	214	1.32	0.74	0.11

Unit of measure is W m^{-2}; n, number of individual (2 hour) budget analyses.

shortwave absorptivity (0.27) and longwave emissivity (0.26) for the aluminum paint which coated the humidity sensor's plastic cap, the possibility of a radiation error cannot be ruled out. The 1915 q depression was larger in the SSA, where solar noon was 1901, than the NSA, where solar noon was 1829 UTC.

4.6. Other Sources of Error

We have neglected daytime radiative heating of the BL; a hypothetical radiative warming rate of 0.04 K h^{-1} over the mean BL depth of 116 hPa would account for a 13 W m^{-2} overestimation of H_s.

A key assumption in the EL budget is that the fluxes are zero at EL top. In fact, EL-top fluxes can be negative for H and positive for λE, when coupled cloud layers cap the BL [*Betts*, 1976]. This would cause H_i and λE_i to be underestimated (in magnitude) and H_s to be biased high and λE_s to be biased low. Comparison with near-surface data from the Twin Otter [*Barr et al.*, this issue] suggests that this may be so. We plan in a subsequent study to attempt stratifications based on the cumulus cloud fraction (which was typically small and, unfortunately, poorly measured) to assess this.

5. Entrainment

5.1. Entrainment Parameterizations

Entrainment is often parameterized in terms of buoyant convection, assuming that the entrainment virtual heat flux at the BL top, H_{vi}, is a constant fraction ($-A_R$) of the surface virtual heat flux H_{vs} [*Betts*, 1973; *Carson*, 1973; *Tennekes*, 1973]:

$$H_{vi} = -A_R H_{vs} \tag{4}$$

The classical value for A_R is 0.20 [*Stull*, 1988], although some recent studies reported mean values for A_R of 0.38 [*Betts et al.*, 1992] or 0.44 [*Betts and Ball*, 1994] above the FIFE grassland, later reduced to 0.31 for no-wind conditions in the work by *Betts and Barr* [1996].

When the influences of wind shear at the surface and BL top are added to (4) [*Stull*, 1976a, 1988; *Tennekes and Driedonks*, 1981],

$$H_{vi} = -\gamma_1 H_{vs} - [\gamma_2 \rho c_p T_0/(gz_i)]u_*^3 - [\gamma_3 \rho c_p T_0/(gz_i)](\Delta u)^3 \tag{5}$$

where ρ (kg m^{-3}) is the density of air, c_p (J kg^{-1} K^{-1}) is the specific heat of air, T_0 (K) is near-surface air temperature, g (m s^{-2}) is the acceleration of gravity, z_i (m) is ML depth, u_* (m s^{-1}) is the friction velocity, and Δu (m s^{-1}) is the "jump" in mean streamwise horizontal wind speed across the EL. The parameters γ_1, γ_2, and γ_3 quantify the combined effects of buoyancy, surface wind shear, and EL wind shear on entrainment. Equation (5) modifies (5) of *Stull* [1976a], using *Stull*'s [1988] assumption that his variable d_1 (the depth of the negative heat flux region in the upper ML) is a constant fraction $A_R/(1 + A_R)$ of ML depth. We incorporated this proportionality into parameters γ_2 and γ_3 in (5).

The value for u_* in (5) was estimated from the mean horizontal wind speed $\langle u \rangle$ in the ML, using the formulae of *Betts and Barr* [1996]. When radiosonde wind speeds were missing (at Thompson before June 7, 1994), $\langle u \rangle$ was estimated from RFE forecasts. In estimating u_*, we used a momentum roughness length z_{0M} of 1.3 m and estimated z as 20% of z_i. The estimates for u_* were sensitive to z/z_{0M}. More seriously, the values of γ_2 and γ_3, in turn, were also dependent upon z/z_{0M} because of the cubic dependence of H_{vi} on u_* in (5). We believe that our values for z/z_{0M}, if anything, have contributed to conservatively low estimates for γ_2 and γ_3.

Table 4. Estimates for Entrainment Parameter A_R, Stratified by Study Area and IFC, With Mean Mixed-Layer Wind Speed $\langle u \rangle$, Friction Velocity u_*, and Entrainment Layer Wind Jump Δu

	Stratification					
	All	SSA	NSA	IFC 1	IFC 2	IFC 3
$\langle u \rangle$, m s^{-1}	5.6	5.5	5.6	5.7	5.1	6.0
u_*, m s^{-1}	0.58	0.58	0.58	0.61	0.53	0.61
Δu, m s^{-1}	0.8	1.1	0.4	0.1	0.9	1.4
A_R	0.21	0.30	0.13	0.15	0.13	0.42
	(0.05)	(0.09)	(0.05)	(0.07)	(0.06)	(0.16)

Values in parentheses are the absolute measurement uncertainties. SSA, southern study area; NSA, northern study area; IFC, Intensive Field Campaign.

5.2. Bulk Estimates of A_R

Table 4 shows our bulk estimates of the entrainment parameter A_R from (5), with an estimate of uncertainty in parentheses, and the mean ML wind speeds and wind shears across the EL. Our value using all data for both study areas and the whole summer is

$$A_R = 0.21 \pm 0.05 \tag{6}$$

This value for A_R is higher than the two estimates of 0.08 $\pm$ 0.12 (composite analysis) and 0.11 $\pm$ 0.10 (mean of individual analyses) derived by *Davis et al.* [this issue] from aircraft measurements of H_{vi} and H_{vs}. As Davis et al. comment, their estimate for A_R has high uncertainty because H_{vi} is estimated by extrapolation from the BL flux profile. Two factors contribute to the uncertainty in A_R: uncertainty in the BL depth and noise in the BL flux profile. Our estimate for A_R lies just within the upper uncertainty limit of the Davis et al. values.

Stratified by study area and IFC, our estimates of A_R show more variability, which we believe is largely a result of the smaller sample size. There is an increase in mean ML wind speed and EL wind shear from IFC 1 to IFC 3, and this may account in some small part for the higher A_R estimate for IFC 3 (see next section). The later sunrise in IFC 3 also means that the 1515–2115 budget period includes more of the rapid ML growth period, when A_R may be high.

It was difficult to quantify the uncertainty in A_R (which we will denote δA_R). Table 4 gives values for δA_R, which were estimated from the observed variability in H_{vi} and H_{vs} (δH_{vi} and δH_{vs}), as

$$|\delta A_R/A_R| = |\delta H_{vi}/H_{vi}| + |\delta H_{vs}/H_{vs}| \tag{7}$$

The values for δH_{vi} and δH_{vs} were estimated from the respective standard errors in H_{vi} and H_{vs}. The variation in $\delta A_R/A_R$ with study area and IFC resulted almost entirely from sample size differences. Considering the wide range and large uncertainty in previous estimates of A_R [*Stull*, 1976b, 1988; *Betts*, 1992], this degree of uncertainty was encouraging. We believe that the degradation in A_R with diminishing sample size re-

Table 5. Estimates for Entrainment Parameter A_R, Stratified by Mean Mixed-Layer Wind Speed $\langle u \rangle$, With Mean Friction Velocity u_* and Entrainment Layer Wind Jump Δu

Stratification	n	$\langle u \rangle$, m s^{-1}	u_*, m s^{-1}	Δu, m s^{-1}	ε_s	β_s	A_R
$\langle u \rangle \leq 4.0$ m s^{-1}	46	2.8	0.41	0.7	0.94	0.90	0.18
4.0 m s^{-1} $< \langle u \rangle \leq 6.0$ m s^{-1}	51	4.9	0.57	0.2	0.85	1.23	0.21
$\langle u \rangle > 6.0$ m s^{-1}	59	8.3	0.83	1.4	1.03	1.00	0.29

Here n is the number of individual (2 hour) budget analyses.

sulted from large random errors in individual 2-hour budgets. The large random errors resulted primarily, not from errors in the radiosonde data, but from the inability of synoptic analyses to resolve local fields of horizontal and vertical advection on a daily or hourly basis. Based on the results of this study, we estimated the minimum number of days required to estimate A_R to within ±40% from sonde-based budget methods to be at least 20.

The neglect of transports out of the BL into shallow clouds in the EL budget biases $|H_{vi}|$ low and $|H_{vi}|$ high, both of which lead to a low bias in A_R, as in the work by *Betts and Barr* [1996].

5.3. Variation of A_R With Wind and EL Wind Shear

We assessed the effects of surface and EL wind shear on A_R by stratifying the budget analyses by friction velocity u_*, mean ML wind speed $\langle u \rangle$, and EL wind speed jump Δu. Tables 5 and 6 show the increase of A_R with increasing $\langle u \rangle$ and Δu stratifications. For both stratifications the increase in A_R was largest between the middle and high classes, consistent with the cubic response of H_{vi} to $\langle u \rangle$ and Δu in (5). (Similar results were found when the data were stratified by u_*.) Our (5) parameter estimates were 0.16 for γ_1, 1.6 for γ_2, and 0.004 for γ_3. We cannot establish clear confidence limits for γ_1, γ_2, or γ_3. However, our estimates are consistent with earlier field and model estimates. Our estimate for γ_1 of 0.16 is a little lower than the accepted value of 0.20 [*Driedonks*, 1982; *Stull*, 1988; *Moeng and Sullivan*, 1994] and much lower than the value of 0.31 from the FIFE grassland [*Betts and Barr*, 1996]. As discussed earlier, the neglect of fluxes at the EL top is a probable cause of a low bias here. The values for γ_2 and, especially, γ_3 were less certain. Our estimate for γ_2 of 1.6 is larger than *Moeng and Sullivan*'s [1994] γ_2 of 1.0. It is also higher than *Betts and Barr*'s [1996] γ_2 of 0.8, but much lower than *Driedonks*' [1982] γ_2 of 5.0 and *Stull*'s [1988] γ_2 of 6.0. Moeng and Sullivan's estimate for γ_2 of 1.0, based on large eddy simulation, is perhaps the most definitive to date. Few previous studies have been able to quantify γ_3. *Moeng and Sullivan* [1994] commented that their entrainment parameterization was unsuited to baroclinic flows because it did not include EL shear. *Driedonks* [1982] found it difficult to obtain accurate data for Δu. Our rough estimate for γ_3 of 0.004 is lower than *Stull*'s [1988] recommended value of 0.0072 but is near the lower end of the γ_3 range (0.0048–0.060) given by *Stull* [1976a].

Table 6. Estimates for Entrainment Parameter A_R, Stratified by the Mean Entrainment Layer Wind Speed Jump Δu, With Mean Mixed-Layer Wind Speed $\langle u \rangle$ and Friction Velocity u_*

Stratification	n	Δu, m s^{-1}	$\langle u \rangle$, m s^{-1}	u_*, m s^{-1}	ε_s	β_s	A_R
$\Delta u \leq 1.5$ m s^{-1}	102	0.0	5.2	0.59	0.92	1.01	0.19
$\Delta u > 1.5$ m s^{-1}	50	2.7	6.5	0.70	1.00	1.29	0.24

Here n is the number of individual (2 hour) budget analyses.

6. Summary and Conclusions

A budget analysis of the 1994 BOREAS radiosonde data has estimated surface fluxes and BL-top entrainment over the boreal forest. Averaged over the summer, this budget estimate of the sum of the surface fluxes, $H_s + \lambda E_s$, underestimated the surface available energy $(R_n - S)$ by only 4%, using an estimate of the landscape energy storage fraction, $S/R_n = 0.17$. For smaller composites of the sonde data, for the two study areas (southern and northern) and three IFCs which spanned late spring to early fall, the sonde budget estimates closed the surface energy balance to within ±13%.

The mean surface Bowen ratio β_s of 1.05 for the boreal forest in summer is much higher than the value of 0.4 over the FIFE grassland [*Smith et al.*, 1992]. The analysis is subject to large random errors, and it was necessary to average the budgets over periods of 15 days or more to produce credible flux estimates. We attributed the errors primarily to the inability of synoptic analyses to resolve local fields of horizontal and vertical advection on a daily or hourly basis.

We also assessed two parameterizations of entrainment over boreal forest. The (4) entrainment parameter A_R was evaluated from sonde-based ML and EL budgets as 0.21, in close agreement with the accepted value of 0.20. Because the EL budget underestimates entrainment, when a cloud layer is coupled to the ML, the value of 0.21 placed a lower limit on A_R.

The value for A_R increased with increasing surface and EL wind shear in a manner similar to previous studies. Stratification by friction velocity and the EL wind speed "jump" gave (5) entrainment parameter estimates of 0.16 for γ_1 (buoyant convection), 1.6 for γ_2 (surface shear), and 0.004 for γ_3 (EL shear). Additional study is needed to assess the impact of shallow clouds and to account for the anomalous near-noon depression in sonde humidity.

Appendix: Relative Humidity Calibration of the Vaisala Radiosonde for BOREAS

A1. Method

A bias in the Vaisala RS80 radiosonde relative humidity (RH) was identified on the basis of laboratory evaluation and routine field checks at the surface before launch. A single bias correction (A1) was applied to the data.

The laboratory evaluation used a General Eastern Hygro

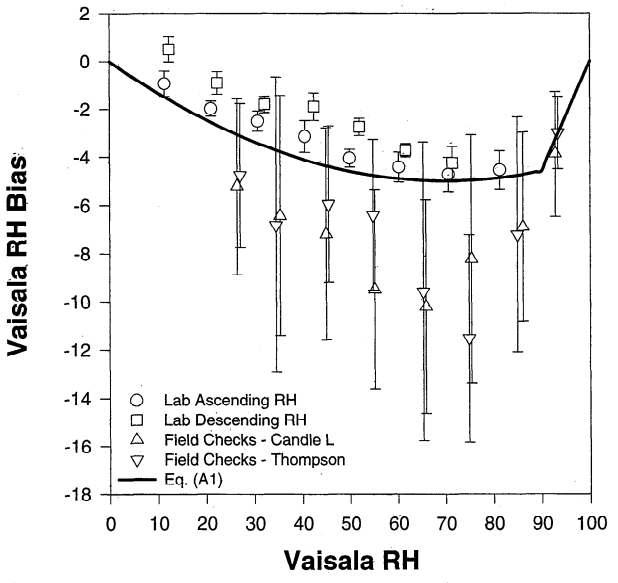

Figure A1. Laboratory and field evaluation of Vaisala RS80 radiosonde relative humidity (RH) calibration, BOREAS 1994. The error bars denote 1 standard deviation from the mean.

M3 dew-point hygrometer, a platinum resistance thermometer, and a General Eastern relative humidity generator. Four sondes were evaluated, drawn from two different batches. The evaluation was at 21°C, and the sondes were powered with 12 V DC. Each sonde was evaluated independently on a separate day. The Vaisala RH sensor was first equilibrated at 15% RH for 60 min. The value for RH was then altered every 20 min in 10% RH steps, ascending from 15% to 85% RH, and then descending from 85% to 15% RH. The value for RH reached equilibrium within 10 min of each step change. Data were sampled and averaged for the final 3 min at each step, at sampling periods of 5 s (M3) and 1.5 s (Vaisala). Field checking was done routinely during the 1994 intensive field campaigns at Candle Lake and Thompson. The field checks used a wet and dry bulb psychrometer in a Stevenson screen, with the sonde hung below the Stevenson screen. The wet-bulb psychrometer was ventilated at Thompson and unventilated at Candle Lake. The computation of relative humidity from wet and dry bulb temperature was done using the standard Atmospheric Environment Service Tables for ventilated and unventilated wet-bulb psychrometers. In addition, a few spot checks were made with a sling psychrometer, and radiation errors were assessed by exposing the temperature and humidity sensors of five sondes to alternating 60 s periods of direct sun and shade.

A2. Results

Figure A1 summarizes the Vaisala RH bias as a function of RH for both laboratory evaluation and field checks. The laboratory evaluation (open circles and squares) of the Vaisala RH sensor showed high precision; a well-defined negative bias, which increased in magnitude from near zero at 15% RH to a maximum of −5% RH at 75% RH (70% Vaisala RH); and a hysteresis of 1% RH after exposure to higher (95%) RH. The Vaisala RH sensors were extremely precise. The standard deviation in the Vaisala RH bias was approximately equal to the RH Vaisala resolution of 1%. The differences between individual sensors were similar at all levels of RH.

The Vaisala RH bias as observed in routine field checks agreed with the laboratory evaluation in sign but was twice as large in magnitude, increasing in magnitude from −5% RH at 27% RH to −10% RH at 70% RH (Figure A1). However, the field-check data were noisy, and the observed bias in the laboratory was most often within 1 standard deviation of the mean field bias. A comparison of the biases observed at Candle Lake and Thompson showed little difference. We cannot adequately explain why the field tests show a larger mean bias. The field data cover a range of temperatures from 4° to 30°C. Radiation errors were small and difficult to detect in the field. The field spot checking of five sondes showed an average shade-to-sun temperature increase of 0.32 ± 0.28°C and an average shade-to-sun RH decrease of −0.16 ± 1.4% RH.

With a conservative philosophy, weighing the laboratory data more heavily, we applied the correction curve (solid line in Figure A1) to the sonde data. This RH bias curve δh is given (as a decimal) by

$$\delta h = \begin{cases} -0.14286h + 0.10204h^2 & h \le 0.9 \\ -0.4592(1 - h) & h > 0.9 \end{cases} \quad \text{(A1)}$$

where h is the Vaisala RH measurement on a 0 to 1 scale. We fitted (A1) to give zero bias at 0 and 100% RH, and a maximum negative bias of 5% at 70% Vaisala RH.

The apparent bias in the Vaisala sonde is a serious one and needs further careful study.

Acknowledgments. The authors acknowledge the work of Chris Winowich, who oversaw the radiosonde field program, and Bob Currie, Jo Lutley, Charles Fenner, and Marlene Webber, who launched the sondes. A.G.B. thanks Charmaine Hrynkiw for help in postprocessing the sonde data; Les Welsh for assistance in retrieving and interpreting RFE model output; and Charmaine Hrynkiw and Bruce Cole for preparing the figures. A.G.B. received support from NASA through the Canadian Centre for Remote Sensing. A.K.B. acknowledges support from NASA under contract NAS5-32356 and NSF under grant ATM-9505018. The radiosonde program was funded by the Atmospheric Environment Service and NASA.

References

Barr, A. G., and G. S. Strong, Estimating regional surface heat and moisture fluxes above prairie cropland from surface and upper-air measurements, *J. Appl. Meteorol.*, *35*, 1716–1735, 1996.

Barr, A. G., A. K. Betts, R. L. Desjardins, and J. I. MacPherson, Comparison of regional surface fluxes from boundary layer budgets and aircraft measurements above boreal forest, *J. Geophys. Res.*, this issue.

Beljaars, A. C. M., and A. K. Betts, Validation of the boundary layer representation in the ECMWF model, in *ECMWF Seminar Proceedings: Validation of Models Over Europe*, vol. II, pp. 159–195, Eur. Cent. for Medium-Range Weather Forecasts, Reading, England, 1993.

Beljaars, A. C. M., P. Viterbo, M. J. Miller, and A. K. Betts, The anomalous rainfall over the USA during July 1993: Sensitivity to land surface parameterization, *Mon. Weather Rev.*, *124*, 362–383, 1996.

Betts, A. K., Nonprecipitating cumulus convection and its parameterization, *Q. J. R. Meteorol. Soc.*, *99*, 178–196, 1973.

Betts, A. K., Reply to comment on the paper "Nonprecipitating cumulus convection and its parameterization," *Q. J. R. Meteorol. Soc.*, *100*, 464–471, 1974.

Betts, A. K., Modeling subcloud layer structure and interaction with a shallow cumulus layer, *J. Atmos. Sci.*, *33*, 2363–2382, 1976.

Betts, A. K., Saturation point analysis of moist convective overturning, *J. Atmos. Sci.*, *39*, 1484–1505, 1982.

Betts, A. K., FIFE atmospheric boundary layer budget methods, *J. Geophys. Res.*, *97*, 18,523–18,531, 1992.

Betts, A. K., and J. H. Ball, Budget analysis of FIFE sondes, *J. Geophys. Res.*, *99*, 3655–3666, 1994.

Betts, A. K., and A. G. Barr, FIFE sonde budget revisited, *J. Geophys. Res.*, *101*, 23,285–23,288, 1996.

Betts, A. K., R. L. Desjardins, and J. I. Macpherson, Budget analysis of the boundary layer grid flights during FIFE 1987, *J. Geophys. Res.*, *97*, 18,533–18,546, 1992.

Betts, A. K., C. S. Bretherton, and E. Klinker, Relation between mean boundary layer structure and cloudiness at the R/V *Valdivia* during ASTEX, *J. Atmos. Sci.*, *52*, 2752–2762, 1995.

Carson, D. J., The development of a dry inversion-capped convectively unstable boundary layer, *Q. J. R. Meteorol. Soc.*, *99*, 450–476, 1973.

Davis, K. J., D. H. Lenschow, S. P. Oncley, C. Kiemle, G. Ehret, A. Giez, and J. Mann, The role of entrainment in surface-atmosphere interactions over the boreal forest, *J. Geophys. Res.*, this issue.

Diak, G. R., and M. S. Whipple, A note on the use of radiosonde data to estimate the daytime fluxes of sensible and latent heat: A comparison with surface flux measurements from the FIFE, *Agric. For. Meteorol.*, *68*, 63–75, 1994.

Driedonks, A. G. M., Models and observations of the growth of the atmospheric boundary layer, *Boundary Layer Meteorol.*, *23*, 283–306, 1982.

Hong, S.-Y., and H.-L. Pan, Nonlocal boundary layer vertical diffusion in a medium-range forecast model, *Mon. Weather Rev.*, *124*, 2322–2339, 1996.

Kustas, W. P., L. E. Hipps, and K. S. Humes, Calculation of basin-scale surface fluxes by combining remotely sensed data and atmospheric properties in a semiarid landscape, *Boundary Layer Meteorol.*, *73*, 105–124, 1995.

Mahrt, L., Mixed layer moisture structure, *Mon. Weather Rev.*, *104*, 1403–1407, 1976.

Mahrt, L., Penetrative convection at the top of a growing boundary layer, *Q. J. R. Meteorol. Soc.*, *105*, 489–485, 1979.

Moeng, C.-H., and P. P. Sullivan, A comparison of shear- and buoyancy-driven planetary boundary layer flows, *J. Atmos. Sci.*, *51*, 999–1022, 1994.

Smith, E. A., et al., Area-averaged surface fluxes and their time-space variability over the FIFE experimental domain, *J. Geophys. Res.*, *97*, 18,599–18,622, 1992.

Stull, R. B., The energetics of entrainment across a density interface, *J. Atmos. Sci.*, *33*, 1260–1267, 1976a.

Stull, R. B., Mixed layer depth model based on turbulent energetics, *J. Atmos. Sci.*, *33*, 1268–1278, 1976b.

Stull, R. B., *An Introduction to Boundary-Layer Meteorology*, 666 pp., Kluwer Acad., Norwell, Mass., 1988.

Tennekes, H., A model for the dynamics of the inversion above a convective boundary layer, *J. Atmos. Sci.*, *30*, 558–567, 1973.

Tennekes, H., and A. G. M. Driedonks, Basis entrainment equations for the atmospheric boundary layer, *Boundary Layer Meteorol.*, *20*, 515–531, 1981.

Teweles, S., A spurious diurnal signal in radiosonde humidity records, *Bull. Am. Meteorol. Soc.*, *51*, 836–840, 1970.

Vaisala, Inc., Solar and infrared temperature correction studies with a special Vaisala RS80 radiosonde, *Vaisala News 128/1992*, Erweko, Helsinki.

Wyngaard, J. C., and R. A. Brost, Top-down and bottom-up diffusion of a scalar in the convective boundary layer, *J. Atmos. Sci.*, *41*, 102–112, 1984.

A. Barr, Atmospheric Environment Service, National Hydrology Research Centre, 11 Innovation Boulevard, Saskatoon, SK, Canada, S7N 3H5. (e-mail: barra@nhrisv.nhrc.sk.doe.ca)

A. K. Betts, Atmospheric Research, RR3 Box 3125, Pittsford, VT 05763.

(Received April 23, 1996; revised January 17, 1997;
accepted February 12, 1997.)